Catalysis Letters Vol. 101, Nos. 3–4, June 2005 (© 2005)
DOI: 10.1007/s10562-005-4899-x

Preparation and characterization of nanosized nickel oxide

Chen-Bin Wang*, Guo-Yuan Gau, Shiue-Jiun Gau, Chih-Wei Tang, and Jia-Lin Bi

Department of Applied Chemistry, Chung Cheng Institute of Technology, National Defense University, Tahsi, Taoyuan, 33509 Taiwan, Republic of China

Received 11 January 2005; accepted 27 January 2005

Nanosized nickel oxide was synthesized by a simple liquid-phase process to obtain the hydroxide precursor and then calcined to form the oxide. The precursor and the nickel oxide were characterized by X-ray diffraction (XRD), infrared spectroscopy (IR), thermal analysis (TG) and temperature-programmed reduction (TPR). The results indicated that the particle size of nickel oxide was controlled by the calcined temperature (T_C). Mixed phases of nickel oxide and nickel hydroxide were present as the T_C was lower than 300 °C. Non-stoichiometric nickel oxide (NiO_x, $x = 1.2$) was formed between 250 °C and 400 °C and a pure nickel oxide was formed as the T_C arrived 500 °C. The particle size of nickel oxide changed as the calcined temperature was controlled under 250 °C, 300 °C, 400 °C and 500 °C, the order was 5.6 nm, 6.5 nm, 11 nm and 17 nm, respectively.

KEY WORDS: nickel oxide; nickel hydroxide; particle size.

1. Introduction

Nanosized materials, such as metal oxides have attracted much attention recently because of their unusual chemical and physical properties which are different from those of bulk materials [1–3]. In particular, nanosized nickel oxides, NiO, are widely used in many technological applications because they exhibit particular catalytic [4,5], anomalous electronic [6,7] and magnetic [8, 9] properties. Another important application of NiO is in a battery system [10,11]. Non-stoichiometric nickel oxide is a good P-type semiconductor owing to its defect structure [12] and it is also a potential gas sensor for H_2 [13]. These applications can be enhanced by decreasing the particle size, preferably to less than 10 nm, and are highly dependent on particle size; the precise control of the size and distribution in a nanometer regime is required.

Techniques for the nano-scale particle preparation have been developed in the last years [14–16]: The chemical routes are widely used to produce a powder product owing to its relative simplicity and its low energy consumption. The present investigation is an attempt towards better controlling the preparation of non-stoichiometric nickel oxide (NiO_x). For this purpose we choose a simple liquid-phase process to obtain the hydroxide precursor and then have it calcined to form the oxide.

In this paper, we report the thermal behavior of $Ni(OH)_2$ and NiO_x particles and the characterization of nanosized NiO_x particles (a controlled size in the 5–20 nm region). To accomplish this work object TG, XRD, IR and TPR are performed to characterize the obtained nickel hydroxide and nickel oxide.

* To whom correspondence should be addressed.
E-mail: chenbin@ccit.edu.tw

2. Experimental

2.1. Catalyst preparation

Nanosized nickel oxide was synthesized by a simple liquid-phase process as follows: Using $Ni(NO_3)_2 \cdot 6H_2O$ as precursor, the 0.6 M solution was heated and kept at 80 °C, then with a magnetic stirring, NH_4OH was added slowly into the solution until pH = 7 was attained. Here a green colloid solution was obtained which was filtered and washed several times with distilled water, then dried at 100 °C for 10 h to obtain the as-prepared precursor, $Ni(OH)_2$ powder. The powder was calcined separately at 250, 300, 400 and 500 °C respectively for 3 h to obtain the nickel oxide.

2.2. Catalyst characterization

X-ray diffraction (XRD) measurements were performed using a MAC Science MXP18 diffractometer with Cu $K_{\alpha 1}$ radiation ($\lambda = 1.5405$Å) at 40 kV and 30 mA with a scanning speed in 2θ of 4° min^{-1}. The crystallite sizes of nickel hydroxide and nickel oxide were estimated using the Scherrer equation.

The infrared spectra were obtained by a Perkin Elmer spectrum GX spectrometer in the range of 1500–4000 cm^{-1}. One milligram of each powder sample was diluted with 200 mg of vacuum-dried IR-grade KBr and subjected to a pressure of 8 tons.

Thermal gravimetric analysis (TG/DTG) was carried out using a Seiko SSC5000 TG system. The rate of heating was maintained at 10 °C min^{-1} and the mass of

the sample was ~10 mg. The measurement was carried from RT to 800 °C under air flowing with a rate of 100 ml min^{-1}.

Reduction behavior of nickel hydroxide and nickel oxide was studied by temperature-programmed reduction (TPR). About 50 mg of the sample was heated in a flow of 10% H_2/N_2 gas mixture at a flow rate of 10 ml min^{-1}. During TPR, the temperature was increased by 7 °C min^{-1} increments from room temperature to 700 °C.

3. Results and discussion

3.1. Characterization of the prepared nickel hydroxide

Figure 1 shows the XRD pattern of the as-prepared precursor, $Ni(OH)_2$. It indicates that all the major peak positions and relative intensities match the JCPDS 14–0117 file identifying β-$Ni(OH)_2$, with a hexagonal structure. The infrared spectrum of the as-prepared precursor is shown in figure 2. The spectrum displays a sharp peak at 3640 cm^{-1} and this confirms that the as-prepared precursor is β-$Ni(OH)_2$ [17]. This sharp peak in the OH stretching vibration is shown by β-$Ni(OH)_2$ because of the absence of hydrogen bonding between hydroxyl groups [18]. In addition to the stretching vibration of the OH bond, other extremely broad, diffuse bands centered around 3450 and 1630 cm^{-1} are assigned to the existence of water.

Figure 3 shows the TG/DTG curves for the decomposition of $Ni(OH)_2$ under a dynamic air (100 ml min^{-1}) environment. The TG curve shows three weight loss steps (assigned as D1, D2 and D3) and the DTG curve shows the maximum loss rate of a D2 step at 280 °C, while both the D1 and D3 steps are not obvious. Prior to 250 °C, the tardy weight loss should be came from desorption of water on $Ni(OH)_2$ surface in heating process. The weight loss of 16% in step D2 is mainly caused by the dehydroxylation of $Ni(OH)_2$ to NiO (theoretical weight loss is 19.4%) and accompanies the oxidation of Ni^{2+} to a higher oxidation state, NiO_x (where x is stoichiometry to be evaluated), according to equations 1 and 2.

$$Ni(OH)_2 \rightarrow NiO + H_2O \quad (1)$$

$$NiO + (x-1)/2O_2 \rightarrow NiO_x \quad (2)$$

$$NiO_x \rightarrow NiO + (x-1)/2O_2 \quad (3)$$

The deviation between an experimental and theoretical value may be the further oxidation of Ni^{2+} to a higher occurrence of an oxidation state. Obviously, only a little amount of the higher oxidation state exists. The weight loss of 4% in step D3 should be caused due to the decomposition of an unstable NiO_x that changed into NiO, as the temperature was above 290 °C according to equation 3. On combining this x value with the weight loss of D2 and D3 in Figure 3, a ~1.2 is therefore estimated.

Figure 4 shows the TPR profile of the as-prepared precursor, $Ni(OH)_2$. The reductive signal of $Ni(OH)_2$ in TPR proceeded by one step at 370 °C according to equation 4.

$$Ni(OH)_2 + H_2 \rightarrow Ni + 2H_2O \quad (4)$$

The ratio of nickel hydroxide species is quantitatively determined from the consumption of hydrogen in TPR traces. The N_{H_2}/N_{Ni} is 1.02.

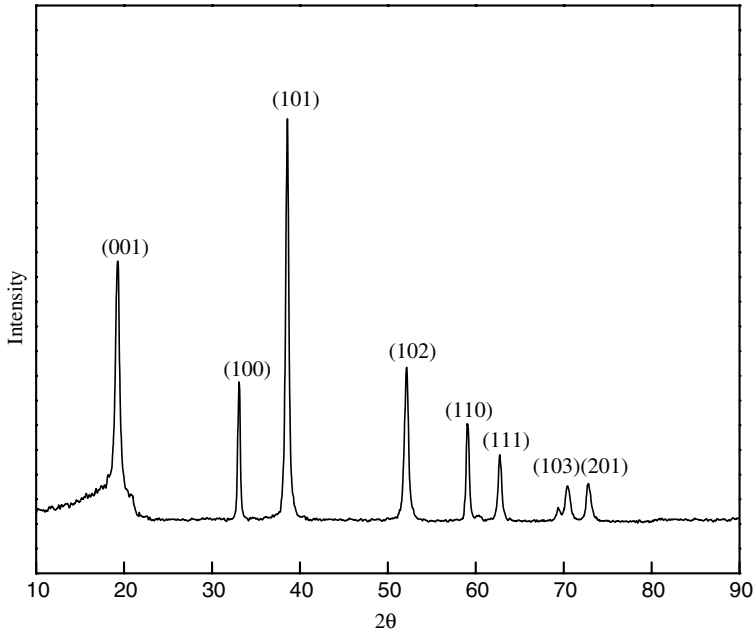

Figure 1. XRD pattern of the as-prepared precursor, $Ni(OH)_2$.

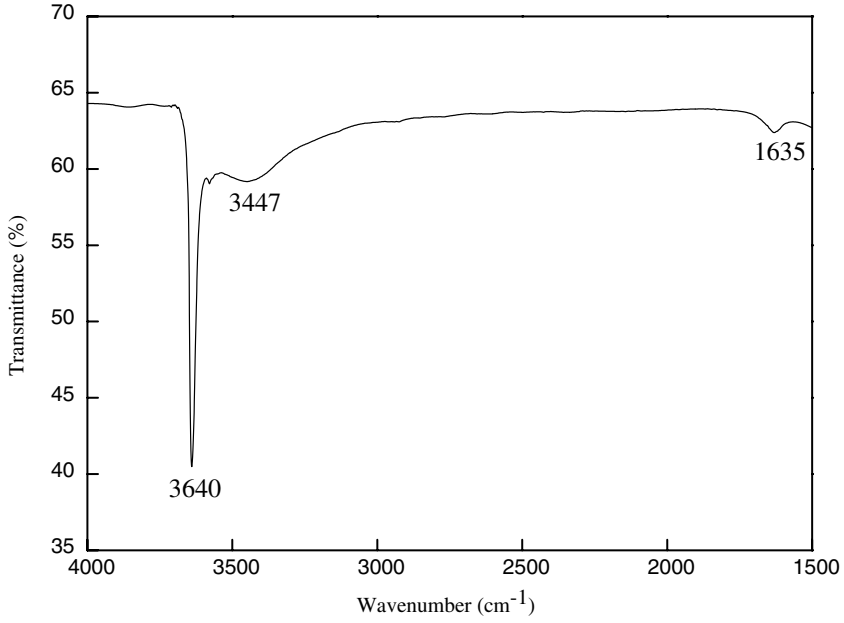

Figure 2. IR spectrum of the as-prepared precursor, $Ni(OH)_2$.

3.2. Characterization of nickel oxide

In order to prepare nickel oxide, four thermal treatments of –250, 300, 400 and 500 °C calcinations from $Ni(OH)_2$ are prepared in flowing air [labeled as C250, C300, C400 and C500], respectively.

Figure 5 presents the XRD patterns of the as-prepared precursor, $Ni(OH)_2$, and the calcined products, NiO_x, at different temperatures. All of the detectable peak positions and relative intensities are consisted from those of the $Ni(OH)_2$ [figure 5(a)] and NiO [figure 5(b)–(e)] phases. The XRD pattern indicates that there is no impurity in the powder. The XRD pattern of the C250 sample [figure 5(b)] presents a weak peak [(101) plane from $Ni(OH)_2$] and overlaps with the (111) plane of NiO. Here, the (101) plane of $Ni(OH)_2$ is not observed when the T_C above 250 °C [figure 5(c)–(e)]. The results show that the $Ni(OH)_2$ converts completely after calcination under air above 250 °C. The same result from the TG analysis demonstrates that the dehydroxylation of $Ni(OH)_2$ occurs at 280 °C.

The mixed phases of the C250 sample can also be observed from an IR and TG analysis. Figure 6 shows the IR spectra of the as-prepared precursor, $Ni(OH)_2$, and the calcined products, NiO_x, at different

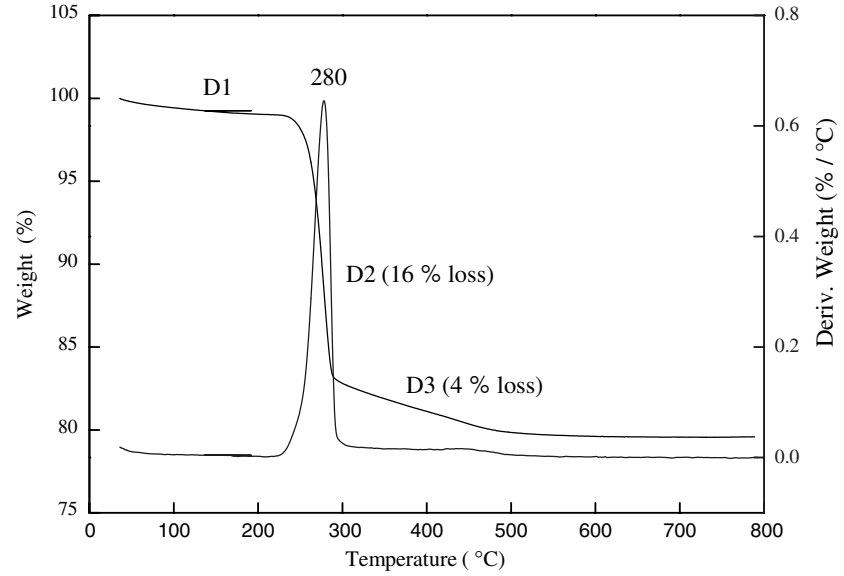

Figure 3. TG/DTG curves for the decomposition of $Ni(OH)_2$ under a dynamic air environment.

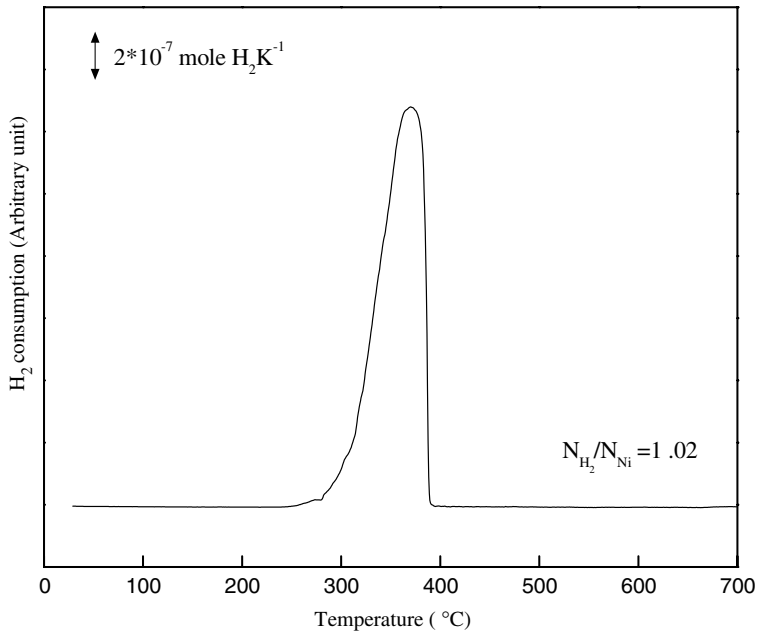

Figure 4. TPR profile of the as-prepared precursor, $Ni(OH)_2$.

temperatures. The C250 spectrum [figure 6(b)] displays a weak peak of v_{OH} stretching at 3633 cm^{-1} and this confirms that the mixed phases exist in a C250 sample. Other thermal treatment samples do not observe v_{OH} stretching [figure 6(c)–(e)]. Figure 7 shows the TG curves of the as-prepared precursor, $Ni(OH)_2$, C250 and C300. Interestingly, the weight loss as attained in step D1 on both C250 and C300 samples [figure 7(b), (c)] is larger than $Ni(OH)_2$. This is likely due to the decomposition of $Ni(OH)_2$ forming NiO through the removal of chemisorbed water (according to equation 1), which necessarily creates more pores to adsorb water under an atmosphere. Also, step D2 is not observed on the C300 sample [figure 7(c)] since the $Ni(OH)_2$ is completely converted to NiO. Whereas step D2 is observed on the C250 sample [figure 7(b)] since the mixed phases of $Ni(OH)_2$ and NiO has been measured with XRD and IR instruments. Weight loss of 2% in step D2 can be evaluated so that the degree of conversion of $Ni(OH)_2$ to NiO is 80% under 250 °C.

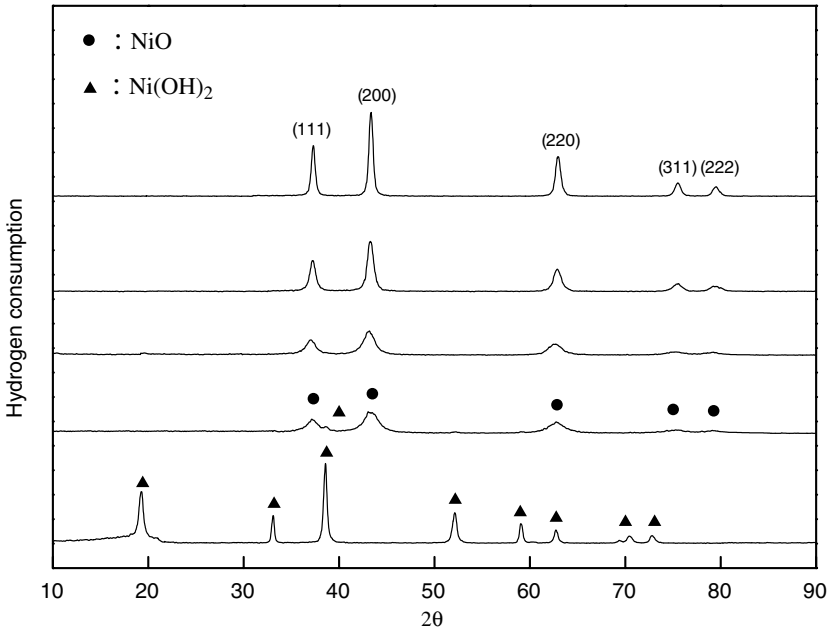

Figure 5. XRD patterns of the as-prepared precursor, $Ni(OH)_2$, and the calcined products, NiO_x, at different temperatures: (a). $Ni(OH)_2$ (b). C250 (c). C300 (d). C400 (e). C500.

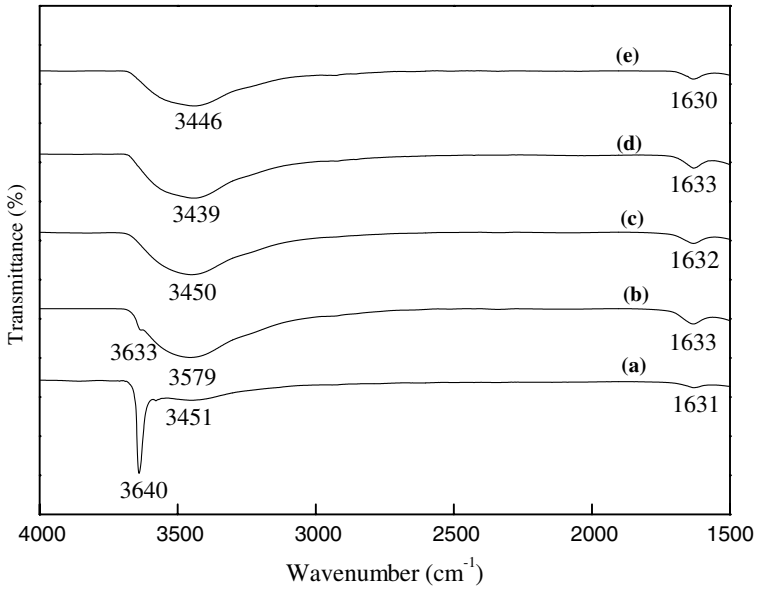

Figure 6. IR spectra of the as-prepared precursor, $Ni(OH)_2$, and the calcined products, NiO_x, at different temperatures: (a). $Ni(OH)_2$ (b). C250 (c). C300 (d). C400 (e). C500.

The effects of the calcination temperature on the crystallite size of NiO particles can be demonstrated from XRD diffraction patterns (figure 5). Traces of NiO crystallite phases (111), (200) and (220) are detected initially in the XRD pattern after calcination at 250 °C, and then their intensities increase symmetrically when the T_C is increased. In general, the sharpness of the XRD peak (i.e. high crystallinity) is increased as the T_C increases. According to the (200) diffraction pattern of NiO crystalline [(101) diffraction pattern for $Ni(OH)_2$], the particle size can be calculated from the full width at half-maximum using the Scherrer equation [19]. Nickel hydroxide and nickel oxide crystallite sizes derived from XRD line broadening analyses after different T_C are given in the 4th column of table 1. Obviously, the particle size of nickel oxide changes as the calcined temperature controlled under 250 °C, 300 °C, 400 °C and 500 °C; the order is 5.6 nm, 6.5 nm, 11 nm and 17 nm, respectively.

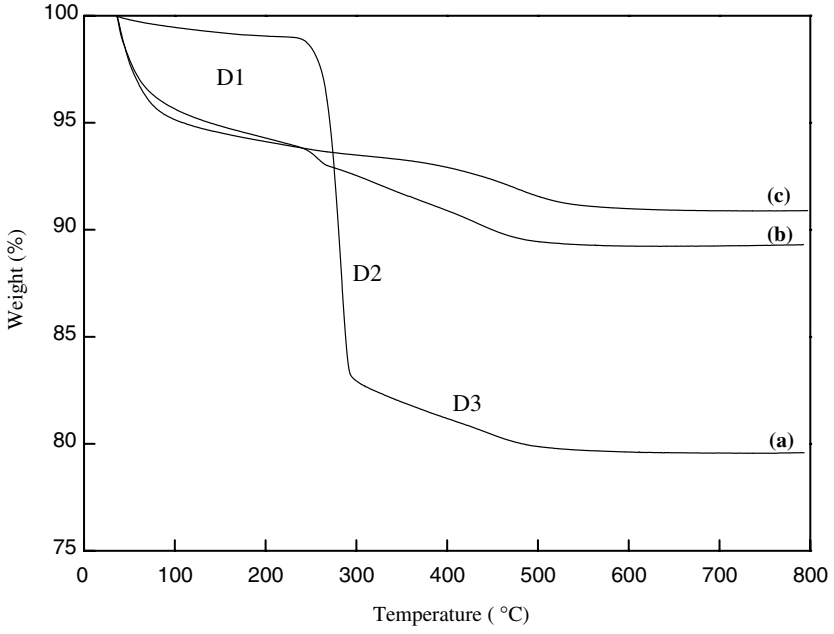

Figure 7. TG curves of the as-prepared precursor, $Ni(OH)_2$, and the calcined products, NiO_x, at different temperatures: (a). $Ni(OH)_2$ (b). C250 (c). C300.

Table 1
Characterization of nickel hydroxide and nickel oxide

Sample	Composition	XRD		FT-IR $v_{O-H}(cm^{-1})$	TPR	
		structure	Particle size(nm)		T_{red}(°C)	N_{H_2}/N_{Ni}
$Ni(OH)_2$ precursor	$Ni(OH)_2$	Hexagonal	22	3640	370	1.02
C250	$Ni(OH)_2$,NiO_x	Cubic	5.6	3633	340	1.19
C300	NiO_x	Cubic	6.5	–	350	1.20
C400	NiO_x	Cubic	11	–	370	1.22
C500	NiO_x	cubic	17	–	400	0.99

Furthermore, the reducibility of the calcination temperature on the crystallite size of NiO particles and the higher oxidation state of nickel oxide are obtained with the qualitative and quantitative TPR technique. Figure 8 displays the TPR profiles of the as-prepared precursor, $Ni(OH)_2$, and the calcined products, NiO_x, at different temperatures. All the samples except $Ni(OH)_2$ and C250 [Figure 8(a), (b)] show a similar TPR profile. The different shape of the TPR profile obtained for C250 [figure 8(b)] is probably due to the mixture of two solid phases (The XRD measurement reveals the existence of $Ni(OH)_2$ and NiO [figure 5(b)]) that affect the shape of the reduction profile. According to the literature [20], the reduction of Ni^{3+} and Ni^{2+} ions to metallic nickel is simultaneous and indistinguishable [Equation (5)].

$$NiO_x + x\ H_2 \rightarrow Ni\ +\ xH_2O \qquad (5)$$

A qualitative analysis of the TPR profile shows that the reduction peak ($T_{red)}$ appears shifted to higher temperatures as the T_C increased [as can be seen in Figure 8 (b)–(e) and the 6th column of Table 1], i.e., the T_{red} of sample C250 is 340 °C [figure 8(b)]. While, the T_{red} of sample C500 is 400 °C [figure 8(e)]. A number of factors can influence reduction, including the particle size of the reducing species [21] and additives [20] used. According to the calculated particle sizes of nickel oxide from XRD [in the 4th column of Table 1], we know that the shift in the T_{red} toward higher temperature is marked more as the particle size increases. The more reducible nickel oxide is located mainly in the small pores with a mean diameters of ~6 nm and the less reducible oxide is located in the larger pores with a mean diameters of ~17 nm. Also, the ratio of nickel oxide species for the calcined products, NiO_x, at different temperature is quantitatively determined from the consumption of hydrogen in TPR traces [list in the last column of table 1]. TheN_H2/N_{Ni} is determined to be 1.19, 1.20, 1.22 and 0.99, respectively, for C250, C300, C400 and C500. This shows that the dominant species upon calcination at 250 ~ 400 °C is NiO_x, where x is larger than 1. As the calcination temperature arrives to 500°C, the decomposition of NiO_x occurs to get a gray colour NiO species ($N_{H_2}/N_{Ni} = 0.99$) which indicates an

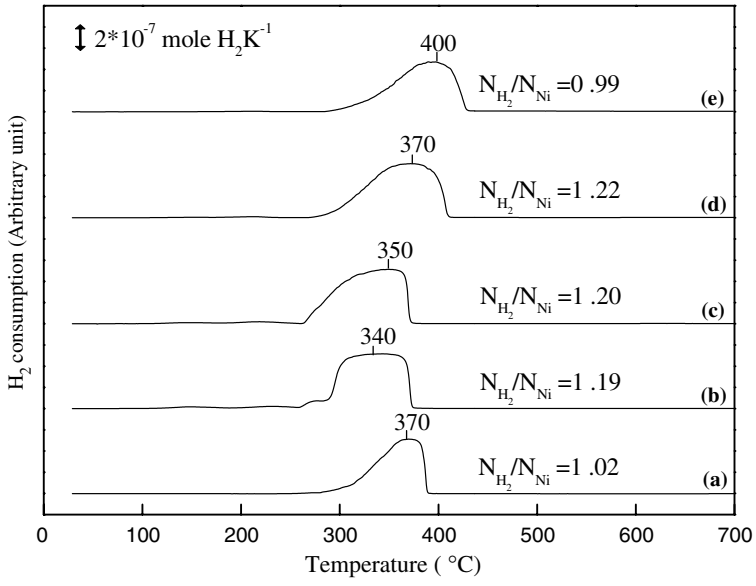

Figure 8. TPR profiles of the as-prepared precursor, $Ni(OH)_2$, and the calcined products, NiO_x, at different temperatures: (a). $Ni(OH)_2$ (b). C250 (c). C300 (d). C400 (e). C500.

efficient departure of non-stoichiometric oxygen. The same tendency is obtained from the TG analysis as can be seen in Figure 3 and Equation (3); the decomposition of NiO_x is in the range of 300 $\sim$ 500°C. So, we confirm that the higher oxidation state of nickel oxide can be obtained under low temperature calcined.

4. Conclusion

This research has shown that high valence nickel oxide ($NiO_{1.2}$) was formed between 300 °C and 500 °C and a pure nickel oxide was formed as the T_C arrived 500 °C. The concentrated results are summarized in Table 1. The following conclusions have been made as follows:

(1) The decomposition of $Ni(OH)_2$ proceeds three consecutive steps, i.e.,

$$Ni(OH)_2 \cdot xH_2O \xrightarrow{T<250^\circ C} Ni(OH)_2 \xrightarrow{T\sim280^\circ C} NiO_x \xrightarrow{T>290^\circ C} NiO$$

(2) The order of particle size is: C500 (17 nm) > C400 (11 nm) > C300 (6.5 nm) > C250 (5.6 nm).

(3) Non-stoichiometric nickel oxide (NiO_x, $x = 1.2$) was formed between 300 °C and 400 °C and a pure nickel oxide was formed as the T_C arrived 500 °C.

Acknowledgments

We are pleased to acknowledge the financial support for this study by the National Science Council of the Republic of China under contract number NSC 93–2113-M-014–003.

References

[1] G. Schmid, Chem. Rev. 92 (1992) 1709.
[2] P.V. Kamat, Chem. Rev. 93 (1993) 267.
[3] K.J. Kjabunde, J. Stark, O. Koper, C. Mohs, G.P. Dong, S. Decker, Y. Jiang, I. Lagadic and D. Zhang, J. Phys. Chem. 100 (1996) 12142.
[4] K.M. Dooley, S.Y. Chen and J.R.H. Ross, J. Catal. 145 (1994) 402.
[5] A. Alejandre, F. Medina, P. Salagre, A. Fabregat and J.E. Sueiras, Appl. Catal. B 18 (1998) 307.
[6] L. Soriano, M. Abbate, J. Vogel and J.C. Fuggle, Chem. Phys. Lett. 208 (1993) 460.
[7] V. Biji and M.A. Khadar, Mater. Sci. Eng. A304–306 (2001) 814.
[8] R.H. Kodama, S.A. Makhlouf and A.E. Berkowitz, Phys. Rev. Lett. 79 (1997) 1393.
[9] R.H. Kodama, J. Magn. Magn. Mater. 200 (1999) 359.
[10] F Li, H. Chen, C. Wang and K. Hu, J. Electroanal. Chem. 531 (2002) 53.
[11] Y. Nuli, S. Zhao and Q. Qin, J. Power Sources 114 (2003) 113.
[12] R. Palombari, J. Electroanal. Chem. 546 (2003) 23.
[13] M. Matsumiya, F. Qiu, W. Shin, N. Izu, N. Murayama and S. Kanzaki, Thin Solid Films 419 (2002) 213.
[14] M.I. Alymov and O.N. Leontieva, Nanostruct. Mater. 6 (1995) 393.
[15] P.L. Llewellyn, V. Chevrot, J. Ragai, O. Cerelier, J. Estienne and F. Rouquerol, Solid State Ionics 101–103 (1997) 293.
[16] J.E. Rodriguez-Paez, A.C. Caballero, M. Villeggas, C. Moure, P. Duran and J.F. Fernandez, J. Eur. Ceramic Soc. 21 (2001) 925.
[17] W.R. Bushing and H.A. Levy, J. Chem. Phys. 26 (1957) 563.
[18] P. Baraldi and G. Davolio, Mater. Chem. Phys. 21 (1989) 143.
[19] H.P. Klug and L.E. Alexander, *X-ray Diffraction Procedures for Polycrystalline and Amorphous Materials*. (Wiley, New York, 1962) 491.
[20] J.T. Richardson, B. Turk and M.V. Twigg, Appl. Catal. A148 (1996) 97.
[21] J.T. Richardson, M. Lei, B. Turk, K. Forster and M.V. Twigg, Appl. Catal. A110 (1994) 217.